Polym. Bull. (2010) 65:227–244
DOI 10.1007/s00289-009-0197-x

ORIGINAL PAPER

N-[2-(8-heptadecenyl)-4,5-dihydro-1H-imidazole-1-ethyl]-2-bromoisobutyramide as initiator for atom transfer radical polymerization (ATRP) and surface-initiated ATRP of methyl methacrylate on iron

Gang Lu · Yi-Min Li · Chun-Hua Lu · Zhong-Zi Xu · Hua Zhang

Received: 12 September 2009 / Revised: 15 October 2009 / Accepted: 16 October 2009 /
Published online: 29 October 2009

Abstract *N*-[2-(8-heptadecenyl)-4,5-dihydro-1H-imidazole-1-ethyl]-2-bromoisobutyramide (IEB) was synthesized and characterized by elemental analysis, FT-IR, and ^{1}H NMR. It had been successfully used as a bidentate initiator for the ATRP of methyl methacrylate with CuBr/2,2′-bipyridine as the catalyst, and *N*,*N*-dimethylformamide as the solvent at 70 °C. The kinetics was first order in monomer and the number-average molecular weight of the polymer increased linearly with the monomer conversion, indicating the 'living'/controlled nature of the polymerization. The polymerization reached high conversions producing polymers with a low molecular weight distribution ($M_w/M_n = 1.319$). The obtained poly(methylmethacrylate) (PMMA) functionalized with 2-(8-heptadecenyl)-4,5-dihydro-1H-imidazoleyl and ω-Br as the end groups were characterized by FT-IR spectroscopy. They can be used as macroinitiators for chain extension reaction. Then, PMMA coatings were grafted from iron substrates by surface-initiated ATRP from a surface-bound IEB initiator. The EIS measurements confirmed the successful grafting of the polymer coatings. Greatly improved short-term anticorrosive properties for PMMA-modified electrodes were demonstrated by substantially increased resistance of the film for a period of 24 h as compared to bare iron.

Keywords Atom transfer radical polymerization · Electrochemical impedance spectroscopy · Imidazole · PMMA-covered iron electrodes · Surface-initiated ATRP

G. Lu (✉) · Y.-M. Li · C.-H. Lu · Z.-Z. Xu · H. Zhang
School of Material Science and Engineering, Nanjing University of Technology, 210009 Nanjing, People's Republic of China
e-mail: lugang3314@163.com

Introduction

One of the most successful polymerization methods in the field of controlled/"living" radical polymerization is atom transfer radical polymerization (ATRP). It is based on the reversible dynamic equilibrium between the active and the dormant species catalyzed by a transition metal complex. ATRP allows the preparation of a wide range of polymeric materials with controlled molecular weights and well-defined architectures [1–8]. Due to its wide uses, intensive investigation has been conducted and large effort has been directed toward the role and the selection criteria of each component of the polymerization mixture (monomer, initiator, transition metal, and ligand) [9, 10].

The initiator is very important because it has to form an initiating radical species via homolytic cleavage of its labile bond such as C–halogen by the catalyst [2]. In early stages, the initiators employed in ATRP were mainly alkyl halides. In 1995, an alkyl chloride (1-phenylethyl chloride, 1-PECl) and carbon tetrachloride (CCl_4) were almost simultaneously reported by Matyjaszewski et al. [2] and Sawamoto et al. [11, 12] Afterward, other organic halides, such as haloketones, haloesters, haloamides, halonitriles, and sulfonyl halides were successfully employed in conventional ATRP [2, 12].

So far, in the area of ATRP, most of the initiators successfully studied are organic halides with a potentially active carbon-halogen bond because fast initiation is vital to obtain well-defined polymers with narrow polydispersities [2]. However, high stabilization of the initiating radical may cause slow initiation, and slow initiation may cause uncontrolled polymerization and high polydispersities polymers; thus, some halogens ($R - X, X = \mathrm{I}$) are not powerful according to the results reported [2, 12]. The other aspect of the initiators is that the initiators used determine the molecular weight of the obtained polymers and its end groups. So the initiator should be selected carefully according to its structure and the catalyst.

In the past few years, imidazole-containing polymers have been widely prepared by living ionic polymerization, due to their attractive chemical properties and their potential use as basic compounds for electrically conducting materials (e.g., solid electrolytes) [13–16]. However, living ionic polymerization requires very strict reaction conditions, which makes it difficult to be performed, and the choice of monomers is quite limited. As discussed above, ATRP not only can provide polymers with controlled molecular weights and narrow polydispersities, but also can be performed using ordinary radical polymerization procedures for various monomers, avoiding the strict conditions needed for living ionic polymerization [2, 17]. Furthermore, functional polymers with low polydispersities and specific end groups can be obtained by using functional initiators in ATRP [18].

An important application of ATRP is the grafting of polymer brushes from the surfaces of flat substrates and colloidal particles. Specially designed surface-attachable ATRP initiators can be immobilized onto the surface, followed by in situ ATRP. An important advantage of this "grafting from" [19–23] method compared to other polymerization grafting methods is the ability to produce polymer brushes with high grafting density.

By grafting polymers with different functionalities, the modified metals become feasible for applications in different areas. For example, by grafting PEG-type [24] or phosphorylcholine-type [25] polymers, the non-specific protein absorptions on metal surfaces can be well prohibited, which is extremely useful for improving the biocompatibility of metal-made bioimplants. Fluoropolymers have a lot of interesting properties, such as high thermal, chemical, and photochemical stability, low refractive index, and low surface energy. The grafting of fluoropolymers makes metal surfaces become "self-cleaning" due to the polymer's excellent water- and oil-repellent properties [26]. The high stability of fluropolymers in all environments can also provide excellent protections to metals from chemical corrosions and photodegradations.

Although there are many different materials that have been successfully used as substrates for surface-initiated ATRP (SI-ATRP) [27–30], some of the most common and important materials in our everyday life, iron, copper, and alloys, have been largely overlooked by the researchers. Unlike other kinds of materials, the surfaces of metals have chemical and physical properties that make them attractive materials for manufacturing. The ability of copper to inhibit the growth of bacteria, viruses, and fungi motivates its use in the fabrication of water pipes and doorknobs. Both metals have excellent electrical and thermal conductivities. As the most efficient conductor of electricity and heat among non-precious metals, copper and iron might be the most extensively used material in electric and electronic devices. Both iron and copper are important components of many important alloys. Despite of all these important applications of iron and copper, no work has been reported on direct grafting of polymers from these two metals.

Therefore, in our work, a new functional initiator *N*-[2-(8-heptadecenyl)-4,5-dihydro-1H-imidazole-1-ethyl]-2-bromoisobutyramide (IEB) was synthesized, and the properties of ATRP of methyl methacrylate (MMA) with this new initiator were investigated under different conditions. Then, PMMA coatings were grafted from iron substrates by SI-ATRP from a surface-bound IEB initiator. The anticorrosive capabilities for the PMMA-modified electrodes were studied by electrochemical impedance spectroscopy in NaCl solutions.

Experiment part

Materials

Methyl methacrylate (MMA)(Chemically Pure, Sinopharm Chemical Reagent Co. Ltd.), triethylamine (Chemically Pure, Shanghai Kaidi Chemical Reagent Co. Ltd.), were purified by vacuum distillation. 2,2′-bipyridine (bpy) (Analytical Reagent, Shanghai Lingfeng Chemical Reagent Co. Ltd.), Tetrahydrofuran (THF) (Analytical Reagent, Shanghai Yishi Chemical Reagent Co. Ltd.), methanol (Analytical Reagent, Sinopharm Chemical Reagent Co. Ltd.), 2-bromoisobutyryl bromide (BiBB) (98%, Acros Organics), *N*,*N*-dimethylformamide (DMF) (Analytical Reagent, Sinopharm Chemical Reagent Co. Ltd.), copper(I) bromide (CuBr) (98%, Acros Organics), methylbenzene (Analytical Reagent, Shanghai Kaidi Chemical Reagent Co. Ltd.),

were used as purchased. 2-(8-Heptadecenyl)-4,5-dihydro-1H-imidazole-1-ethylamine (OLC) and distilled water was self-made.

Synthesis of IEB

2-(8-Heptadecenyl)-4,5-dihydro-1H-imidazole-1-ethylamine (OLC) was synthesized by referring to a procedure in literature [31, 32]. In a 200-mL flask equipped with a reflux condenser and a dropping funnel, there were placed 24 g of DETA and 50 mL of dimethylbenzene, and the reaction mixture was kept at 140 °C with magnetically stirring. OAI was dropped during 60 min to the solution through the dropping funnel, which was stirred for 2 h at 140 °C. After the water carried out from the solution with dimethylbenzene in the first step of dehydration, the temperature quickly increased to 180 °C for an additional 2 h. Until there is no water carried out by dimethylbenzene, the resulting solution was purified by vacuum distillation, the product was OLC. Then, a 100 mL of flask with a magnetic stirrer was purged with nitrogen for 10 min, OLC (8 g, 23 mmol), triethylamine (6 mL), methylbenzene (12 mL) was added after the flask was cooled to 0 °C using ice/water bath. Then the solution of BiBB (3 mL, 24 mmol, 8 mL methylbenzene) was added slowly for 2 h via a syringe and a yellow precipitate formed immediately. After BiBB was added completely, the reaction persisted for 24 h at 0 °C. The reaction mixture was extracted with distilled water to remove the amine salt. At last, the solvent methylbenzene and residual triethylamine were removed under vacuum, the final product was IEB.

Polymerization of MMA via ATRP

The general procedure of the polymerization was as follows: CuBr (0.068 g), bpy (0.1473 g), MMA (10 mL), and *N*,*N*-dimethylformamide (10 mL, 50% v/v) were added to an ampule tube under stirring, three cycles of vacuum-nitrogen were applied in order to remove the oxygen. After the catalyst was dissolved (about 10 min), EBP (0.06 mL) was added via a syringe. Then the ampule tube was sealed under nitrogen and placed in a water bath thermostated at the desired temperature. Aliquots were taken and placed into an ice bath to stop the reaction periodically via syringes to follow the kinetic of the polymerization process. The aliquots were diluted with THF followed by filtration through a basic alumina column prior to PMMA isolated by precipitation in methanol and dried in vacuum at 25 °C for 24 h.

Surface-initiated ATRP (SI-ATRP) of MMA on iron coupons

The 1 cm thick iron coupons were polished sequentially up to 1,200 grit SiC paper. The newly polished coupons were washed with copious amounts of deionized water, acetone, ethanol, and deionized water, in that order, for 5 min each to degrease and clean the surface. Then, freshly cleaned iron coupons were immersed in a 2.5 mg/mL DMF solution of IEB for 12 h at room temperature for self-assembly. The modified

coupons were rinsed with copious amount of deionized water to remove unattached initiator and dried under a stream of dry N_2. For the preparation of PMMA brushes on the iron surface, MMA (10 ml), CuBr (0.068 g), and bpy (0.1473 g) was added together, and then the iron coupons were introduced into the reaction mixture under N_2 protection. The reaction tube was sealed and kept in 70 °C water bath to produce iron–PMMA surfaces. After 1, 3, 5 h, the coupons were removed from the reaction tube and were quickly rinsed with deionized water and dried under N_2.

Characterization

Conversion of monomer was determined by gravimetry. Number-average molecular weights and molecular weight distributions of polymers obtained were measured using a Waters 515 GPC, equipped with microstyragel column (HR1, HR3, HR4) with THF as a mobile phase at a flow rate of 1 cm^3/min operated at 25 °C. Linear polystyrene standards were used for calibration. ^1H NMR spectra was recorded in deuterated chloroform ($CDCl_3$) using tetramethylsilane (TMS) as internal reference on a BmemerAv400 spectrometer at ambient temperature. FT-IR spectra was using MAGNA-IR 750 (Nicolet Instrument Co. USA) model FT-IR spectrometer in the 4,000–400 cm^{-1} region by dispersing the sample in KBr discs. The complex was characterized by the elemental analyses using Vario El-III CHNSO elemental analyzer (Elementar Co. Germany).

Electrochemical measurements

To assess the anticorrosion properties of the surface-functionalized coupons of iron (self-assembled IEB monolayers and iron–PMMA), impedance spectra was used. The pristine and the surface-functionalized coupons were mounted in a PVDF holder, leaving a circular area of 1 cm^2, to serve as the working electrode. The cell for electrochemical measurements was a traditional three-electrode cell. The working electrode was iron electrode, a platinum wire was used as a counter electrode, and the reference electrode was a saturated calomel electrode (SCE). The working electrode was facing downward while the counter electrodes were placed vertically facing each other. The reference electrode was led to the surface of the working electrode through a Luggin capillary. The impedance measurements were performed 0.5 h after the electrode had been immersed in the electrolyte. The electrochemical measurements were performed with IM6 electrochemical workstation (ZAHNER, Germany). Impedance measurements were performed under free corrosion potential (E_{corr}) with a sinusoidal potential perturbation of 10 mV in amplitude and frequency from 100 kHz to 10 mHz. The data of impedance spectra were fitted to probable equivalent circuits using the program ZVIEW (version 3.0, Scribner Associates, Inc.). Potentials reported in this article were all referred to SCE, and the solution was 0.5 mol/L NaCl solution.

Result and discussion

Synthesis and characterization of the new initiator

N-[2-(8-heptadecenyl)-4,5-dihydro-1H-imidazole-1-ethyl]-2-bromoisobutyramide (IEB), as shown in Scheme 1, could be easily obtained. IEB was a kind of *N*-heterocyclic compound containing alkyl bromide group, so it can be used for ATRP as initiator. The new initiator was checked using elemental analysis, FT-IR spectra, and ^{1}H NMR spectra.

Analytical results of the composition of IEB of carbon, hydrogen, nitrogen were given in Table 1. The results agreed well with the calculated value and were consistent with the proposed structure.

In the ^{1}H NMR spectrum of the initiator (Fig. 1), all the signals corresponding to the proposed structure were observed in $CDCl_3$. The methyl protons (number 1) were assigned at $\delta = 0.86$ ppm. The protons (number 2) were observed at $\delta = 5.33$ ppm. The proton (number 3) on the imidazole ring appeared at $\delta = 3.61$ ppm. The methylene protons (number 4) were observed at $\delta = 2.31$ ppm. The proton of acidamide (number 5) was assigned at $\delta = 6.70$ ppm. But it was not so obvious. The peaks at $\delta = 2.01$ ppm was ascribed to molar contributions of the methyl protons (number 6).

FT-IR spectra of IEB (Fig. 2) exhibited the characteristic absorptions between 1,590–1,610 cm^{-1}(C=N stretching of imidazole ring); 2,920–2,940 cm^{-1} (C–H stretching of imidazole ring); 3,300–3,400 cm^{-1} (N–H stretching of acidamide); 1,680–1,690 cm^{-1} (C=O stretching of acidamide); 1,280–1,300 cm^{-1} (C–N stretching of acidamide); 2,850–2,870 cm^{-1} (C–H stretching of methyl); 990–1,010 cm^{-1} (=C–H stretching); 620–640 cm^{-1} (C–Br stretching). The data above illustrated that the product was confirmed to be *N*-[2-(8-heptadecenyl)-4,5-dihydro-1H-imidazole-1-ethyl]-2-bromoisobutyramide (IEB) exactly.

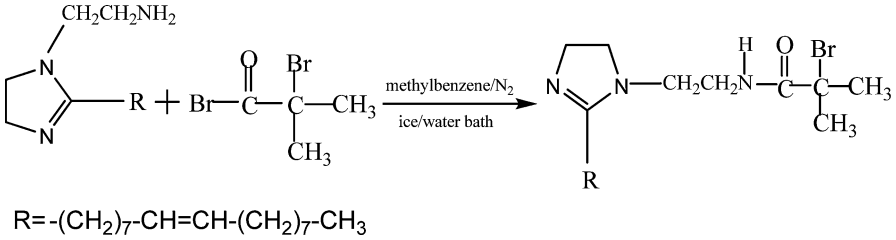

Scheme 1 Synthesis of the new initiator

Table 1 Elemental analysis results of IEB

IEB	% N	% C	% H
Found	8.37	63.22	9.43
Calculated	8.43	62.65	9.64

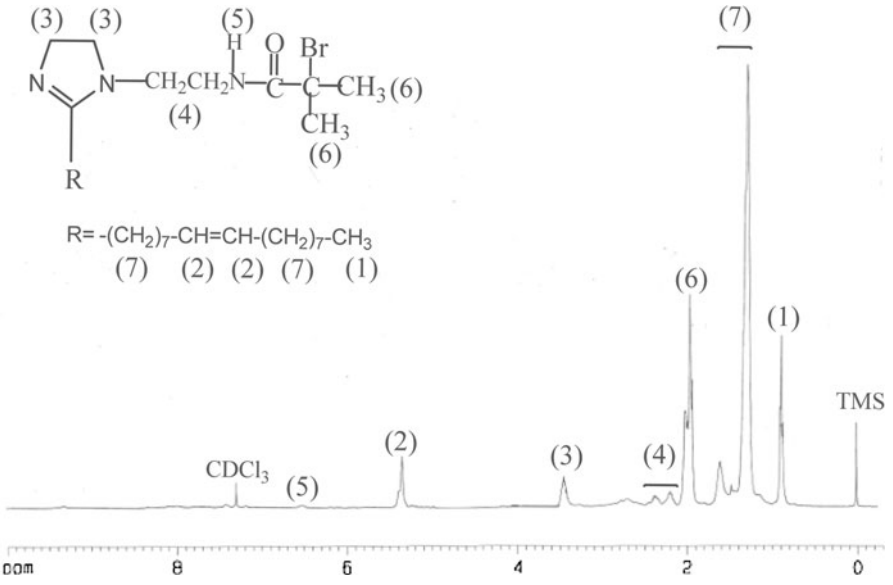

Fig. 1 ^{1}H NMR spectrum of the new initiator IEB in $CDCl_3$

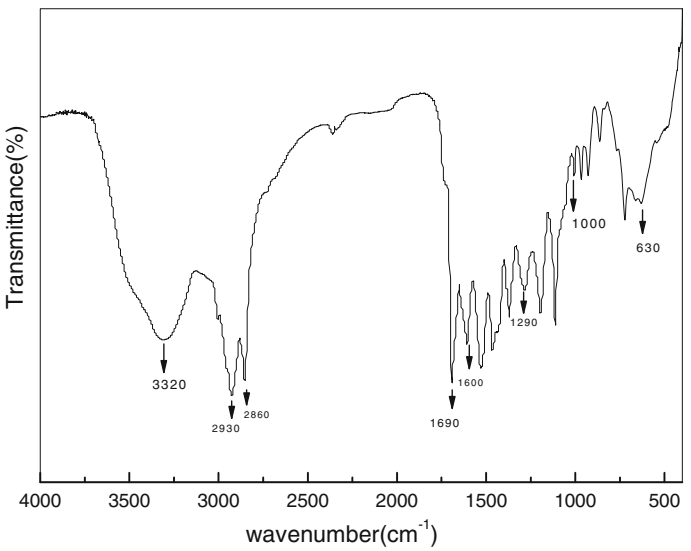

Fig. 2 FT-IR spectrum of IEB

ATRP of MMA with the new initiating system

Polymerization of MMA with the condition of $[MMA]_0$:$[IEB]_0$:$[CuBr]_0$:$[bpy]_0 = 200:1:1:2$ was carried out in DMF at 70 °C. The polymerization reached 69.90% within 4 h at 70 °C to yield PMMA of $M_n = 18860$ and $M_w/M_n = 1.32$.

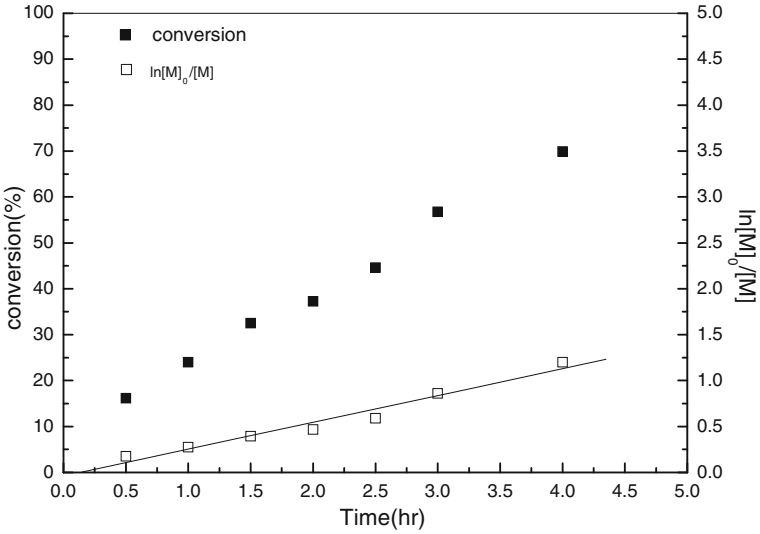

Fig. 3 Plots of conversion and $\ln[M]_0/[M]$ versus time for the ATRP of MMA initiated by IEB in DMF at 70 °C, $[MMA]_0$:$[IEB]_0$:$[CuBr]_0$:$[bpy]_0$ = 200:1:1:2, DMF: 50% v/v

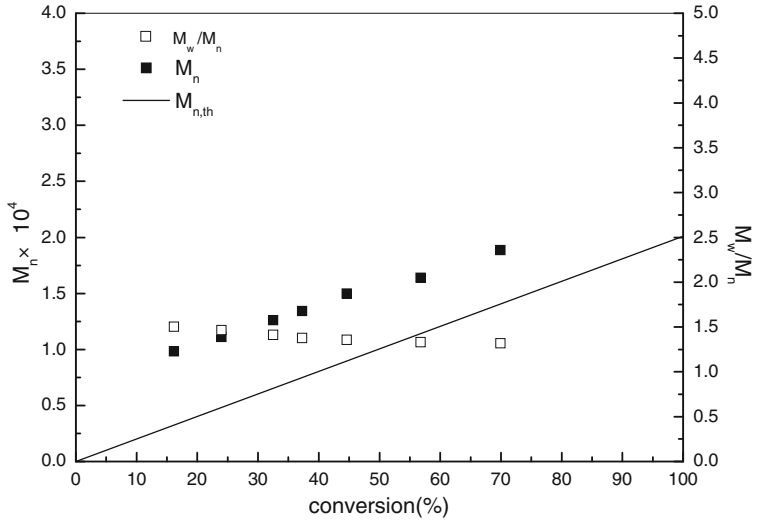

Fig. 4 Molecular weight (M_n) and molecular weight distribution (M_w/M_n) dependence on monomer conversion for the polymerization of MMA under the same conditions as in Fig. 3

The linear dependence of $\ln[M]_0/[M]$ on reaction time indicated that the kinetics were first order in monomer and that the living radical concentrations were during the polymerization process, as observed from Fig. 3. From the same figure, it also can be seen that the monomer conversion increased with the reaction time. Figure 4 showed that the experimental molecular weights increased linearly with monomer conversion

with quite narrow polydispersity index (1.32–1.50), indicating the absence or an insignificant amount of transfer reaction. However, the experimental molecular weights were higher than the calculated ones ($M_{n,th}$), which were calculated as $M_{n,th} = [monomer]_0/[initiator]_0 \times conversion \times M_{monomer} + M_{initiator}$. The efficiencies ($f$) of initiator, calculated as $f = M_{n,th}/M_{n,GPC}$ were relatively low (0.38–0.77). At the beginning of the polymerization (<10% conversion), there might have been too many primary radicals produced from the decomposition of IEB, which could not become dormant species by halogen transfer and underwent termination by combination reactions.

Chain extension reaction

If the chain end was a bromine atom, a recovered PMMA should be able to initiate the polymerization of a fresh feed of MMA in the presence of a classical ATRP system. To confirm the activity, we carried out the chain extension polymerization of MMA using PMMA as macroinitiator ($M_n = 18{,}860$, $M_w/M_n = 1.32$) prepared via ATRP with $[MMA]_0:[IEB]_0:[CuBr]_0:[bpy]_0 = 200:1:1:2$ at 70 °C. The chain extension was conducted with fresh MMA and the component ratio $[MMA]_0:[\text{recovered PMMA}]_0:[CuBr]_0:[bpy]_0 = 2000:1:10:20$ at 70 °C in DMF (50% v/v). After 12 h, the conversion reached 32.33% with $M_n = 36{,}760$ and $M_w/M_n = 1.47$ (Fig. 5a). The increase in the molecular weight indicated that the chain ends of the obtained macroinitiator were functionalized. However, the final PMMA had a little higher M_w/M_n, which might be due to that the macroinitiator did not participate in the reaction. Since the GPC trace contained a notable shoulder, resulting from original PMMA, it was possible to deconvolute the GPC trace via peak splitting. The peak splitting technique allowed the obtained GPC trace of the various reaction products to be split into its constituent traces. The result of the peak splitting using a Gaussian deconvolution of the obtained GPC trace of PMMA displayed that the area ratio of chain extension PMMA and original PMMA was 0.93 and 0.07 (Fig. 5b).

End group analysis

In order to gain insight into the nature of this new initiating system, the structure of the polymer $P_{MMA\text{-}Br}$ synthesized by the IEB/CuBr/bpy system was analyzed using FT-IR spectrometer and ^{1}H NMR spectrometer. In Fig. 6, the characteristic absorptions were obtained between 1,610–1,630 cm^{-1}(C=N stretching of imidazole ring); 2,910–2,930 cm^{-1} (C–H stretching of imidazole ring); 3,400–3,450 cm^{-1} (N–H stretching of acidamide); 1,720–1,740 cm^{-1} (C=O stretching of ester group); 1,100–1,120 cm^{-1} and 1,150–1,170 cm^{-1} (C–O–C stretching of ester group); 2,840–2,860 cm^{-1} (C–H stretching of methyl); 1,040–1,060 cm^{-1} (=C–H stretching). In Fig. 7, the methyl protons (number 1 and 2) were assigned at $\delta = 3.71$ and $\delta = 0.84$ ppm. The protons (number 3) were observed at $\delta = 1.81$ ppm. These signals were corresponding to the MMA. The proton (number 3) on the imidazole ring appeared at $\delta = 3.61$ ppm. The other signals were attributed to IEB. These results, including the success of chain extension with the ATRP initiating system (Fig. 5),

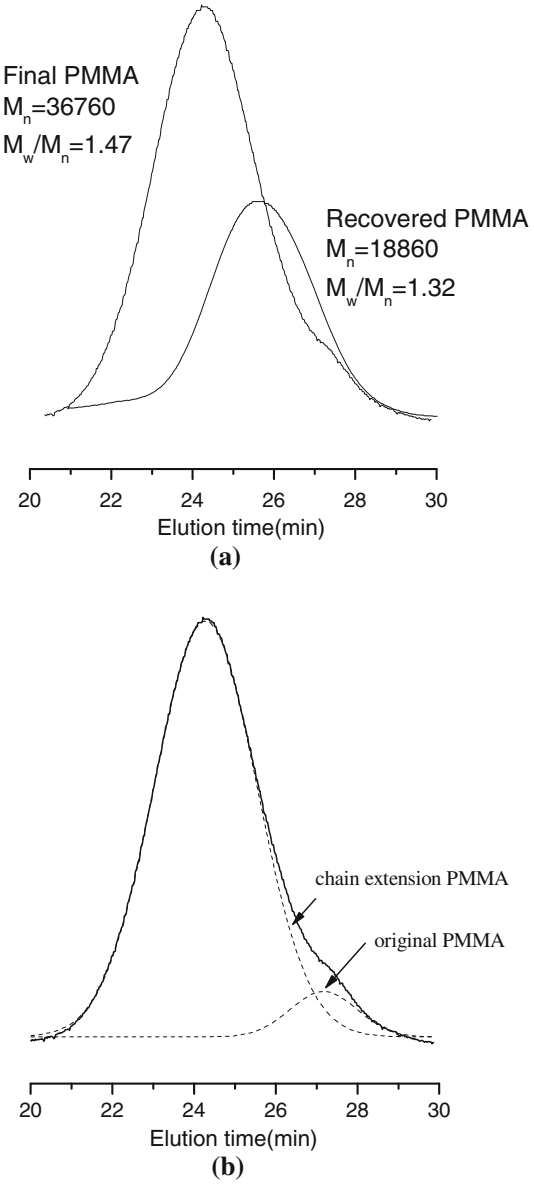

Fig. 5 **a** GPC curves of polymers (recovered PMMA and final PMMA) after chain extension of PMMA synthesized by IEB/CuBr/bpy. **b** Deconvolution of GPC trace of the PMMA via peak splitting

thus confirmed that the polymer had 2-(8-heptadecenyl)-4,5-dihydro-1H-imidazoleyl and ω-Br as the end groups and the polymerization should undergo an ATRP process.

Electrochemical impedance spectroscopy (EIS)

Measurements were performed to determine the impedance parameters of the naked-iron/electrolyte, IEB monolayers-covered iron/electrolyte, or PMMA-covered iron/

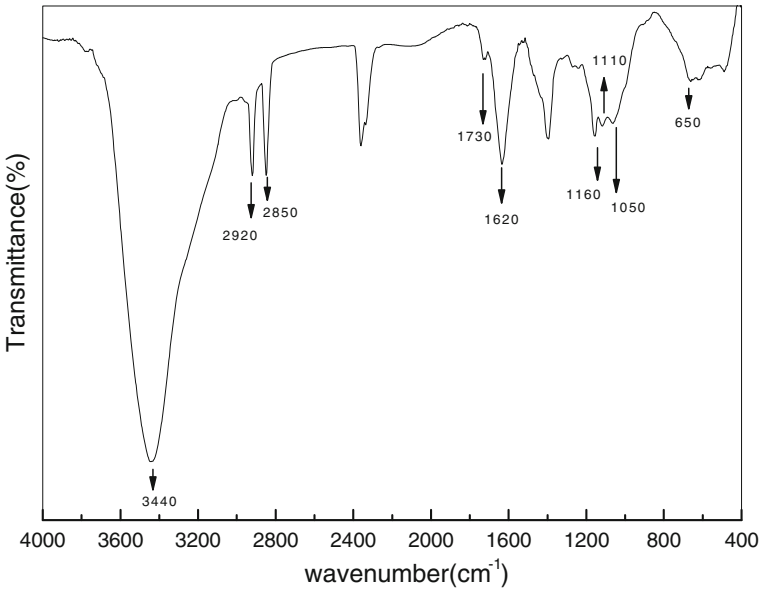

Fig. 6 FT-IR spectrum of the ω-Br end group of PMMA initiated with IEB/CuBr/bpy ($[MMA]_0$:$[IEB]_0$:$[CuBr]_0$:$[bpy]_0$ = 200:1:1:2) at 70 °C. Sample: $M_{n(PMMA\text{-}Br)}$ = 18,860, M_w/M_n = 1.32

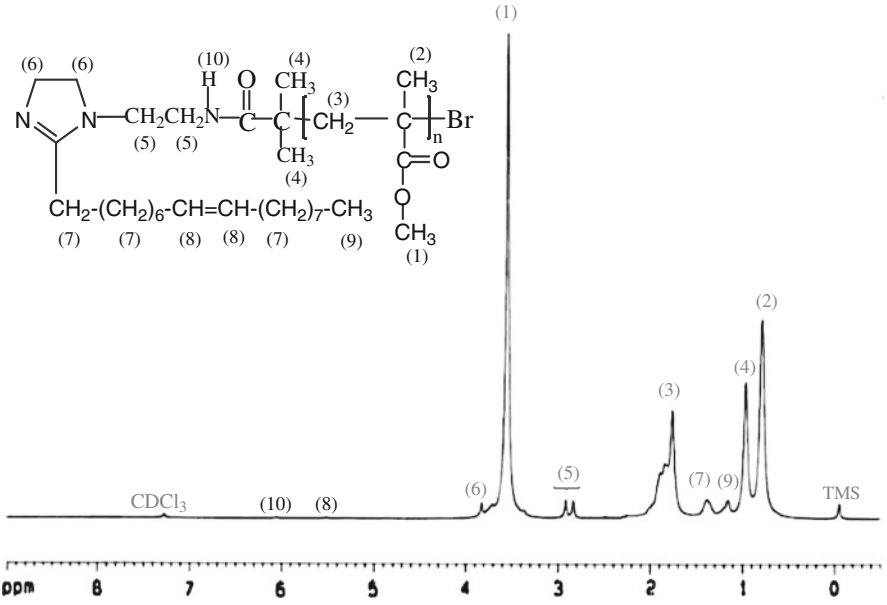

Fig. 7 ^{1}H NMR spectrum of the ω-Br end group of PMMA initiated with IEB/CuBr/bpy ($[MMA]_0$:$[IEB]_0$:$[CuBr]_0$:$[bpy]_0$ = 200:1:1:2) at 70 °C. Sample: $M_{n(PMMA\text{-}Br)}$ = 18,860, M_w/M_n = 1.32

electrolyte. Figure 8 was the Nyquist impedance spectroscopy for the naked-iron and IEB self-assembled monolayers (SAMs) covered electrodes in 0.5 mol/L NaCl solution.

The Nyquist plot of naked-iron measured in NaCl solution (see Fig. 8a) displayed an obvious capacitive loop deviating from an ideal semicircle in high frequency, which was bought by surface roughness and was known as the "dispersing effect", and a straight line (Warburg impedance) in low frequency. The capacitive loop was attributed to the relaxation time constant of the charge-transfer resistance (R_{ct}) whose value was approximately equal to the diameter of the capacitive loop and the double-layer capacitance (C_{dl}) at the iron/electrolyte interface [33], and the Warburg impedance was due to diffusion of soluble reactant or product species [34]. Considering that the impedance of a double layer did not behavior as an ideal capacitor in the presence of a dispersing effect, a constant phase element of double layer (CPE_{dl}) was used as a substitute for the capacitor to fit more accurately the impedance behavior of the electric double layer. It had been calculated that the value of R_{ct} was 790 Ω cm^2 using Zview impedance software. In the NaCl solution, the corrosion reaction at iron surface consisted of the anodic dissolution of copper and the cathodic reduction of the dissolved oxygen. Recent study showed that the diffusion process was controlled by diffusion of dissolved oxygen from the bulk solution to the electrode surface and the Warburg impedance was ascribed to the diffusion of oxygen [35].

The impedance spectra of IEB monolayer covered iron electrodes were quite different from that of nake- iron electrodes. In NaCl corrosive solution, the Warburg impedance observed previously in Fig. 8a disappeared, and only a depressed semicircle with diameter of more than 2.23×10^3 Ω cm^2 was observed.

Figure 9 was the Nyquist impedance spectra of iron electrode covered with different molecular weight of PMMA films in 0.5 mol/L NaCl solution. The exposure time in NaCl solution and the molecular weight of PMMA were changed to investigate the inhibitive efficiency. The impedance spectra of PMMA-covered electrodes were different from that of the naked-iron electrodes both in size and shape. Compared with the Nyquist spectroscopy of naked-iron electrode, the diameter size of the semicircle of PMMA-covered iron electrode tended to be larger.

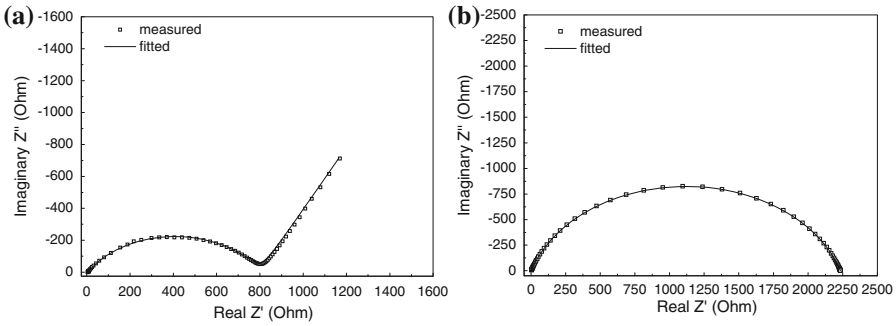

Fig. 8 Nyquist impedance spectroscopy of **a** the naked-iron electrode and **b** the IEB SAMs-covered iron electrode in 0.5 mol/L NaCl solution

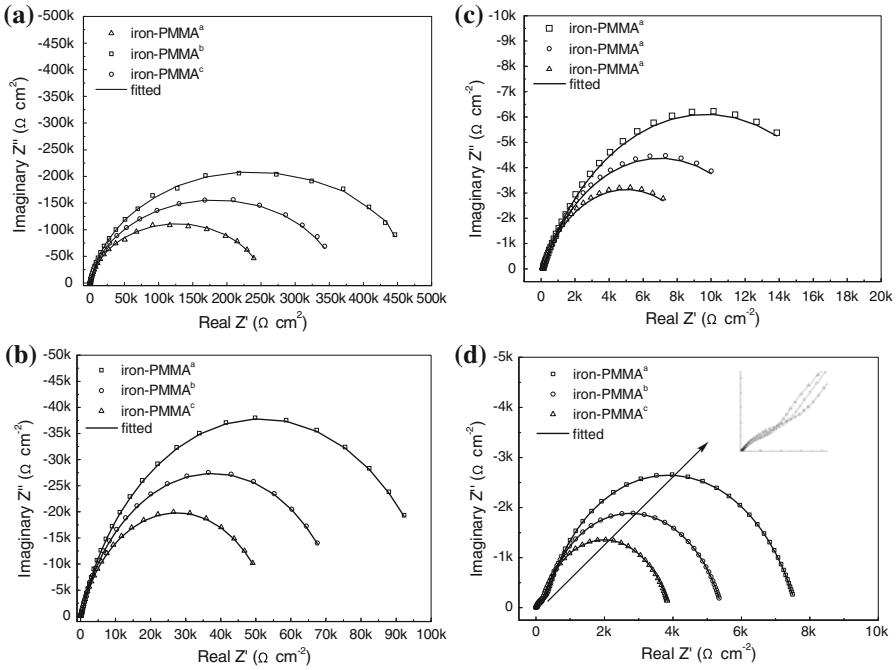

Fig. 9 The variation of impedance spectroscopy for the PMMA-covered iron electrode with different molecular weight of PMMA under different immersion time in 0.5 mol/L NaCl solution: **a** 1 h, **b** 3 h, **c** 7 h, and **d** 24 h. [a]The M_n of PMMA is 6.683×10^5. M_w/M_n is 1.43. The polymerization time is 5 h. [b]The M_n of PMMA is 4.232×10^5. M_w/M_n is 1.48. The polymerization time is 3 h. [c]The M_n of PMMA is 1.667×10^5. M_w/M_n is 1.55. The polymerization time is 1 h

It was found from Fig. 9 that with the increasing of molecular weight of PMMA, the diameter size of the semicircle of PMMA-covered iron electrode tended to be larger, and with the exposure time extending, the diameter size of the semicircle became smaller. The larger diameters of the semicircle indicated the decreasing in corrosion rate of iron electrode under the protection of polymer layer. When the time reached 24 h, the impedance spectra gave two poor-separated capacitive loops whose diameters were reduced with exposure time (Fig. 9d). The appearance of a low capacitive loop for long immersion times indicated the occurrence of electrochemical corrosion reaction. It was mean that the polymer coating was damaged or degraded, and the aggressive ions and water penetrated though polymer coating and reacted with metal substrate, giving rise to the expansion of the defective sites, and leading to further destruction of polymer coating.

Different equivalent circuits (ECs) [36] have been established so far to interpret impedance behavior of the electrodes. However, these circuits are inconsistent with each other in interpreting the physical meaning of elements and explaining the origin of impedance loops. In this study, three ECs were proposed to model the respective impedance spectra of the naked and the surface-functionalized iron electrodes (Fig. 10). EC (a) is used to fit the impedance spectra of coupons with a compact surface film, EC (b) is used to model the impedance spectra of coupons

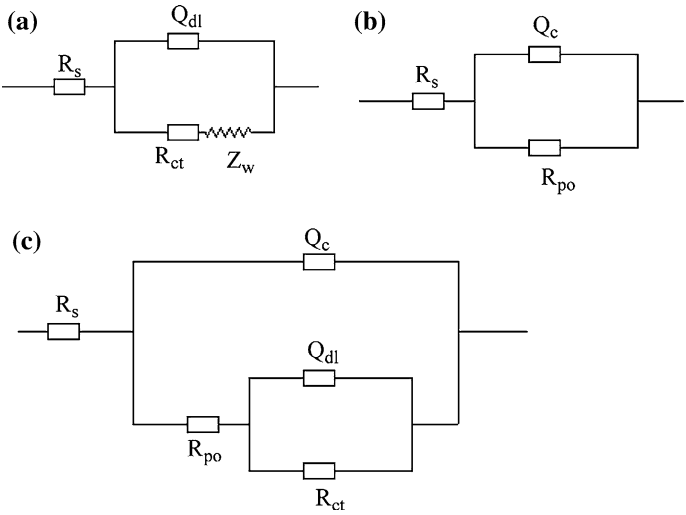

Fig. 10 Equivalent circuits to fit the EIS for iron displaying **a** a Warburg impedance, **b** one capacitive loop, and **c** two capacitive loops

with porous and non-protective surface film, while EC (c) has been widely used to estimate the barrier, protection, and degradation of the polymer coatings.

In Fig. 10, R_s is the solution resistance between the working electrode and reference electrode; R_{ct} is the charge-transfer resistance corresponding to the corrosion reaction at metal substrate/solution interface; Q_{dl} is constant phase elements modeling the double-layer capacitance; Z_w, the Warburg impedance attributes to mass transport in the process of corrosion reactions; the pore resistance (R_{po}) represents the extent of ionic conduction through a polymer in an electrolytic environment, and is commonly used as a criterion for assessing the extent of corrosion protection derived from the organic coatings, while the constant phase elements (CPE) of coating, Q_c, is used to substitute coating capacitance, C_c, by taking into account of the phenomena related to the heterogeneous surface and diffusion process.

The fitted parameters of the impedance spectra were summarized in Table 2. The quality of PMMA films can be evaluated by R_{po} and Q_c [37]. The more densely packed the layers, the larger the R_{po} values and the lower the C_c values. Value of n for the Q_c element can be used as an index to determine whether PMMA films behaved like a capacitor. The behavior of SAMs tended to be an ideal capacitor when value of n approaches $+1$ gradually.

From the data, it can be seen that the value of the charge-transfer resistance of the naked-electrode was the lowest. When the surface of iron electrodes were covered with IEB films, the value of R_{ct} increased. In the case of the PMMA-covered iron, R_{po} values were significantly large, indicative of the decrease in corrosion rate under the protection of polymer layer. On the other hand, R_{po} and R_{ct} values increase with the enhancement of M_n of PMMA films, indicative of the substantial increased in barrier property of the polymer coating against the penetration of aggressive ions

Table 2 Fitting parameters of the EIS spectra for iron in 0.5 mol/L NaCl solution

	Exposure time (h)	R_s (Ω cm^2)	R_{ct} (Ω cm^2)	Q_{dl}		R_{po} (Ω cm^2)	Q_c		Z_w (Ω cm^2)
				C_{dl} (F cm^{-2})	n		C_c (F cm^{-2})	n	
Naked-iron	–	4.97	0.79×10^3	7.13×10^{-3}	0.648	–	–	–	1.46×10^{-3}
IEB Monolayers on iron		2.73	2.23×10^3	1.1×10^{-6}	0.814	–	–	–	–
Iron–PMMA[a]	1	9.90	–	–	–	4.79×10^5	5.41×10^{-5}	0.91	–
Iron–PMMA[b]		7.86	–	–	–	3.65×10^5	6.61×10^{-5}	0.90	–
Iron–PMMA[c]		6.45	–	–	–	2.56×10^5	7.60×10^{-5}	0.90	–
Iron–PMMA[a]	3	13.01	–	–	–	1.03×10^5	1.30×10^{-4}	0.79	–
Iron–PMMA[b]		11.22	–	–	–	7.62×10^4	1.76×10^{-4}	0.80	–
Iron–PMMA[c]		8.69	–	–	-	5.41×10^4	2.31×10^{-4}	0.81	–
Iron–PMMA[a]	7	11.06	–	–	–	1.86×10^4	1.02×10^{-3}	0.75	–
Iron–PMMA[b]		9.79	–	–	–	1.43×10^4	1.32×10^{-4}	0.71	–
Iron–PMMA[c]		7.88	–	–	–	9.82×10^3	1.88×10^{-4}	0.73	–
Iron–PMMA[a]	24	6.24	7.00×10^3	1.76×10^{-4}	0.87	0.61×10^3	1.12×10^{-4}	0.71	–
Iron–PMMA[b]		9.32	5.13×10^3	2.03×10^{-4}	0.83	0.44×10^3	1.33×10^{-4}	0.66	–
Iron–PMMA[c]		5.09	3.58×10^3	2.57×10^{-4}	0.82	0.32×10^3	1.64×10^{-4}	0.69	–

[a] The Mn of PMMA is 6.683×10^5. Mw/Mn is 1.43. The polymerization time is 5 h

[b] The Mn of PMMA is 4.232×10^5. Mw/Mn is 1.48. The polymerization time is 3 h

[c] The Mn of PMMA is 1.667×10^5. Mw/Mn is 1.55. The polymerization time is 1 h

and water. However, it can be seen that the longer the immersion time was, the smaller the values R_{po} and n were. This indicated that the behavior of PMMA films was deviating gradually from a pure capacitor with extending the immersion time. The capacitance (Q_c) of coating as a function of exposure time in an electrolyte solution provided information on stability of the coating and the extent of water uptake. Q_c increased gradually with exposure time, indicative of the uptake of the electrolyte and water by the polymer coatings, and thus the decrease in protective capability of the polymer coating.

Conclusion

A new *N*-heterocyclic initiator containing imidazole group (IEB) was synthesized and utilized in ATRP of MMA with CuBr/2,2′-bpy as the catalyst and DMF as the solvent. With this new initiating system, the number-average molecular weights of polymers increase with increasing monomer conversion and the kinetics are first order in monomer. M_w/M_n of PMMA was as low as 1.32, but the initiator efficiency is not high. The obtained well-defined PMMA functionalized with 2-(8-heptadecenyl)-4,5-dihydro-1H-imidazoleyl and ω-Br, as the end groups were characterized by FT-IR spectroscopy and used as macroinitiators for chain extension reaction. Then, PMMA coatings were grafted from iron substrates by SI-ATRP from a surface-bound IEB initiator. The EIS measurements confirmed the successful grafting of the polymer coatings. Greatly improved short-term anticorrosive properties for PMMA-modified electrodes were demonstrated by substantially increased resistance for a period of 24 h as compared to bare iron.

Acknowledgment We gratefully acknowledge the support of this work by the Analysis Center of China Pharmaceutical University.

References

1. Nanda AK, Matyjaszewski K (2003) Effect of [bpy]/[Cu(I)] ratio, solvent, counterion, and alkyl bromides on the activation rate constants in atom transfer radical polymerization. Macromolecules 36:599–604
2. Matyjaszewski K, Xia J (2001) Atom transfer radical polymerization. Chem Rev 101:2921–2990
3. Percec V, Barboiu B (1995) 'Living' radical polymerization of styrene initiated by arenesulfonyl chlorides and CuI(bpy)nCl. Macromolecules 28:7970–7971
4. Wang JS, Matyjaszewski K (1995) 'Living'/controlled radical polymerization. Transition-metal-catalyzed atom transfer radical polymerization in the presence of a conventional radical initiator. Macromolecules 28:7572–7573
5. Teodorescu M, Matyjaszewski K (2000) Controlled polymerization of (meth)acrylamides by atom transfer radical polymerization. Macromol Rapid Commun 21:190–194
6. Wang G, Zhu XL, Cheng ZP, Zhu J (2005) Atom transfer radical polymerization of styrene initiated by the novel initiator 2-bromo-2-nitropropane. E-polymers no. 035
7. Tang W, Matyjaszewski K (2007) Effects of initiator structure on activation rate constants in ATRP. Macromolecules 40:1858–1863
8. Wang G, Zhu XL, Cheng ZP, Zhu J (2003) Reverse atom transfer radical polymerization of methyl methacrylate with $FeCl_3$/pyromellitic acid. Eur Polym J 39:2161–2165

9. Zhu C, Sun F, Zhang M, Jin J (2004) Atom transfer radical suspension polymerization of methyl methacrylate catalyzed by CuCl/bpy. Polymer 45:1141–1146
10. Nanda AK, Matyjaszewski K (2003) Effect of [PMDETA]/[Cu(I)] ratio, monomer, solvent, counterion, ligand, and alkyl bromide on the activation rate constants in atom transfer radical polymerization. Macromolecules 36:1487–1493
11. Kato M, Kamigaito M, Sawamoto M, Higashimura T (1995) Polymerization of methyl methacrylate with the carbon tetrachloride/dichlorotris-(triphenylphosphine)ruthenium(II)/methylaluminum bis(2,6-di-tert-butylphenoxide) initiating system: possibility of living radical polymerization. Macromolecules 28:1721–1723
12. Kamigaito M, Ando T, Sawamoto M (2001) Metal-catalyzed living radical polymerization. Chem Rev 101:3689–3745
13. Arslan A, Kıralp S, Toppare L, Bozkurt A (2006) Novel conducting polymer electrolyte biosensor based on poly(1-vinyl imidazole) and poly(acrylic acid) networks. Langmuir 22:2912–2915
14. Zhu AH, Wang Z, Xie MR, Zhang YQ (2007) Synthesis of imidazole end-capped poly(n-butyl methacrylate)s via atom transfer radical polymerization with a new functional initiator containing imidazolium group. E-Polymers no. 009
15. He XY, Yang W, Pei XW (2008) Preparation, characterization, and tunable wettability of poly(ionic liquid) brushes via surface-initiated atom transfer radical polymerization. Macromolecules 41:4615–4621
16. Rannard SP, Davis NJ, Herbert I (2004) Synthesis of water soluble hyperbranched polyurethanes using selective activation of AB(2) monomers. Macromolecules 37:9418–9430
17. Matyjaszewski K, Wang JL, Grimaud T, Shipp DA (1998) Controlled/'living' atom transfer radical polymerization of methyl methacrylate using various initiation systems. Macromolecules 31:1527–1534
18. Coessens V, Pintauer T, Matyjaszewski K (2001) Functional polymers by atom transfer radical polymerization. Prog Polym Sci 26:337–377
19. Roy D, Semsarilar M, Guthire JT, Perrier S (2009) Cellulose modification by polymer grafting: a review. Chem Soc Rev 38:2046–2064
20. Nguyen S, Marchessault RH (2005) Atom transfer radical copolymerization of bacterial poly(3-hydroxybutyrate) macromonomers and methyl methacrylate. Macromolecules 38:290–296
21. Advincula RC, Btittain WJ, Caster KC (2005) Polymer brushes. Wiley, New York
22. Prucker O, Ruhe J (1998) Mechanism of radical chain polymerizations initiated by azo compounds covalently bound to the surface of spherical particles. Macromolecules 31:602–613
23. Prucker O, Ruhe J (1998) Synthesis of poly(styrene) monolayers attached to high surface area silica gels through self-assembled monolayers of azo initiators. Macromolecules 31:592–601
24. Fan XW, Li LJ, Dalsin JL, Messersmith PB (2005) Biomimetic anchor for surface-initiated polymerization from metal substrates. J Am Chem Soc 127:15843–15847
25. Feng W, Brash JL, Zhu SP (2005) Adsorption of fibrinogen and lysozyme on silicon grafted with poly(2-methacryloyloxyethyl phosphorylcholine) via surface-initiated atom transfer radical polymerization. Langmuir 21:5980–5987
26. Granville AM, Brittain WJ (2004) Stimuli-responsive semi-fluorinated polymer brushes on porous silica substrates. Macromol Rapid Commun 25:1298–1302
27. Patten TE, Xia J, Abernathy T, Matyjaszewski K (1996) Polymers with very low polydispersities from atom transfer radical polymerization. Science 272:866–868
28. Jordan R, Ulman A (1999) Surface-initiated anionic polymerization of styrene by means of self-assembled monolayers. J Am Chem Soc 121:1016–1022
29. Zhao B, Brittain WJ (2000) Polymer brushes: surface-immobilized macromolecules. Prog Polym Sci 25:677–710
30. Chen RX, Zhu SP, Maclaughlin S (2008) Grafting acrylic polymers from flat nickel and copper surfaces by surface-initiated atom transfer radical polymerization. Langmuir 24:6889–6896
31. Szyprowski AJ (2000) Relationship between chemical structure of imidazoline inhibitors and their effectiveness against hydrogen sulphide corrosion of steels. Br Corro J 35:155–160
32. Bistline RG, Hampson JW, Linfield WM (1983) Synthesis and properties of fatty imidazolines and their N-(2-aminoethyl) derivatives. J Am Oil Chem Soc 60:823–828
33. Barcia OE, Matoos OR (1990) Reaction model simulating the role of sulphate and chloride in anodic dissolution of iron. Electrochim Acta 35:1601–1608

34. Ma H, Chen S, Niu L, Shang S, Zhao S, Li S, Quan ZJ (2001) Studies on electrochemical behavior of copper in aerated NaBr solutions with Schiff base, N,N-*o*-phenylen-bis(3-methoxysalicylidenimine). J Electrochem Soc 148:B208–B216
35. Ma H, Chen S, Niu L, Zhao S, Li S, Li D (2002) Inhibition of copper corrosion by several Schiff bases in aerated halide solutions. J Appl Electrochem 32:65–72
36. Zamborini FP, Crooks RM (1998) Corrosion passivation of gold by n-alkanethiol self-assembled monolayers: effect of chain length and end group. Langmuir 14:3279–3286
37. Feng Y, Teo WK, Siow KS, Gao Z, Tan KL, Hsieh AK (1997) Corrosion protection of copper by a self-assembled monolayer of alkanethiol. J Electrochem Soc 144:55–64